Compensation of the Effects of Antenna Dispersion on UWB Waveforms via Optical Pulse-Shaping Techniques

Jason D. McKinney, *Member, IEEE*, and Andrew M. Weiner, *Fellow, IEEE*

***Abstract*—To our knowledge, we present the first experimental demonstration of compensation of antenna dispersion effects on impulsive ultra-wideband (UWB) signals. By extracting the RF spectral phase from a time-domain impulse response measurement of a pair of ridged TEM horn antennas, we utilize a photonic-synthesis technique for arbitrary electromagnetic signal waveforms to generate a signal ''matched'' to the antenna pair. We demonstrate that the received waveform is compressed and exhibits reduced ringing levels, as compared to the impulse response of the system. Our technique is reprogrammable and we believe the technique will be applicable to a variety of antennas operating in the UWB communications band of 3.1–10.6 GHz.**

***Index Terms*—Antenna dispersion, RF photonics, ultra-wideband (UWB) signal generation.**

I. Introduction

THE FIELD of microwave photonics, where optical techniques are utilized to increase RF systems performance, has seen significant growth in the past several years. In particular, the use of photonics to transmit or measure RF waveforms has seen particular research emphasis. For example, radio-over-fiber links [1] and photonic analog-to-digital conversion [2], [3] have clearly demonstrated photonics as an enabling technology for these RF applications. Photonic techniques for RF and microwave signal synthesis, as well as systems employing these techniques, are far less common.

The majority of research on photonically synthesized electromagnetic signals has emphasized waveforms in the millimeter frequency range. Specifically, optical heterodyne techniques have been used to generate narrowband signals in the ~12–37-GHz range [4] and optical pulse-shaping techniques have been utilized to generate burst and continuous waveforms in the ~30–50-GHz range [5]. With the ever increasing interest in ultra-wideband (UWB) applications such as impulse radio [6] and ground-penetrating radar [7], optical techniques for synthesis of UWB waveforms with frequency content in the Federal Communications Commission-specified 3.1–10.6-GHz UWB band [8] are extremely desirable—yet are very limited in number. The predominant technique is the use of Fourier transform optical pulse shaping combined with optical frequency-to-time conversion in a dispersive medium and subsequent optical-to-electrical (O/E) conversion. This technique has been demonstrated for the creation of chirped sinusoids [9], as well as a variety of broadband sinusoidal and impulsive RF waveforms [10]. Though all of the above photonic techniques have demonstrated capabilities outside of those offered by purely electronic signal generation instrumentation, few have found application in RF and microwave systems.

An area where photonic techniques could significantly impact RF systems, particularly UWB wireless systems, is in compensation of signal distortion—e.g., distortions experienced by impulsive waveforms during radiation from broadband antennas. Given the broad frequency bandwidth available to UWB wireless systems, it is desirable for the antennas in these systems to exhibit an ideal frequency response over the 3.1–10.6-GHz UWB band. Such an idealized response—consisting of a flat frequency response and linear phase delay—is, functionally, rarely achieved [11], [12]. Though some antenna structures, such as the TEM horn and Vivaldi antennas, do exhibit relatively flat frequency responses and relatively linear phase [13], most other structures show a nonlinear spectral phase response at a minimum. Therefore, methods to compensate for nonideal antenna behavior through design and implementation of optimized UWB waveforms are necessary.

Methods to compensate for phase errors (both temporal and spatial) introduced by an antenna or array have been widely explored. Specifically, the concept of optimizing the antenna feed voltage to obtain desirable temporal properties in the received waveform—such as peak voltage amplitude or minimal received pulsewidth—have been explored in detail for dipole antennas [14]. This concept has also been extended to dipole arrays with extra constraints (e.g., on the sidelobe level of the far-field radiation pattern), and illustrates that the input excitation waveform may be tailored to optimize both temporal and spatial properties of the signal radiated from the array [15]. With regard to UWB systems, there has been significant theoretical interest in waveform optimization to combat antenna and channel distortions (specifically dispersion) in recent years. With respect to antenna phase response, it has been shown that the transmit waveform may be designed to optimize the received waveform in UWB systems, e.g., to maximize the received voltage amplitude or minimize the received voltage pulsewidth [16]. Though the effects of antenna phase distortions (dispersion) on UWB signals are readily observed and optimization techniques have been proposed to mitigate such distortions [16], to our knowledge there have been no experimental demonstrations of these techniques.

Manuscript received August 1, 2005; revised January 10, 2006. This work was supported by the Army Research Office under Contract DAAD19-03-1-0275.

The authors are with the School of Electrical and Computer Engineering, Purdue University, West Lafayette, IN 47907-2035 USA (e-mail: mckinnjd@purdue.edu).

Digital Object Identifier 10.1109/TMTT.2006.871999

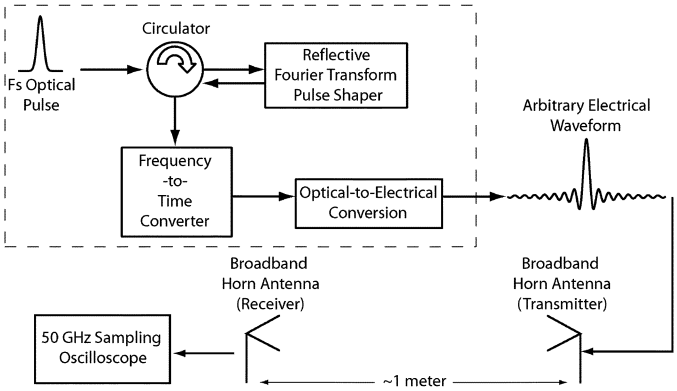

Fig. 1. Experimental apparatus. Our photonic time-domain electromagnetic waveform generator comprises the components inside the dashed line.

In this study, we present a technique based on photonic arbitrary electromagnetic waveform generation for UWB signal synthesis that allows the transmit waveform to be pre-compensated for antenna dispersion. Through time-domain impulse response measurements, we extract the RF spectral phase contributed by broadband ridged TEM horn antennas to signals transmitted over a wireless link and apply the conjugate spectral phase to our transmit waveform to achieve signal compression at the receiver. We demonstrate the received waveform in our system is indeed compressed and exhibits reduced duration and secondary oscillations as compared to the antenna link impulse response. We believe our technique and waveform generation apparatus form an enabling technology for a variety of UWB systems.

II. Experiment

A. Photonic Time-Domain Electromagnetic Signal Generation

A schematic of our experimental apparatus is shown in Fig. 1. Our antennas are ridged TEM horn antennas (Dorado International GH1-12N) with a specified bandwidth of 1–12 GHz. The output of the photonic time-domain electromagnetic signal generator is amplified with a broadband microwave amplifier (0.1–18 GHz, ∼29-dB power gain) and used as the input to the transmit antenna. A second identical antenna is positioned 1-m away and functions as the receiver. The output of the second antenna is measured on a 50-GHz sampling oscilloscope. The distance of 1 m was chosen to satisfy the far-field constraint of $2D^2/\lambda$ at a frequency of 1 GHz and the antenna height (∼1 m) was chosen to ensure any multipath components were clearly resolvable. Here, our use of highly directional antennas and efforts to avoid multipath interference emphasize the line-of-sight link response. For this response, distortions of the received waveform will arise from the response of our antennas, not the channel. This allows us to address the antenna response independent of the channel (multipath or nonline-of-sight reception).

At the core of our apparatus is a technique for synthesis of arbitrary RF and microwave waveforms based on ultrafast optical arbitrary waveform technology [9], [10]. Our apparatus consists of a mode-locked femtosecond fiber laser, Fourier transform optical pulse shaper [17], optical frequency-to-time converter, and O/E converter, as shown in Fig. 1. Ultrashort optical pulses from an erbium fiber laser (∼100 fs, 50-MHz repetition rate) are spectrally filtered in a reflective-geometry Fourier transform optical pulse shaper. This pulse shaper enables impression of a user-defined optical filter function onto the spectrum of the optical pulse. After exiting the pulse shaper, these short pulses are dispersed in 5.5 km of single-mode optical fiber (Corning SMF-28). The chromatic dispersion of the fiber uniquely maps optical frequency to time; thus, after exiting the fiber, the temporal optical intensity is a scaled version of the filter function applied in the optical pulse shaper. Subsequent to the fiber, these tailored optical intensity waveforms are converted to electrical signals via O/E conversion by a 60-GHz photodiode. After O/E conversion, the electrical waveform then also exhibits the shape of the optical filter function applied in the optical pulse shaper. This enables user-defined time-domain electrical waveforms to be directly specified, as illustrated in [10].

A detailed description and the operational specifics of our apparatus are given in [10]. Here, we will simply describe the relevant parameters. The time aperture of our apparatus is 3 ns and is determined by the optical bandwidth and length of the fiber stretcher. The minimum temporal feature size is limited by the resolution of our optical pulse shaper and frequency-to-time conversion constant of the fiber stretcher to approximately 45 ps; the resulting RF bandwidth is ∼11 GHz. We note that the time aperture and temporal resolution may be configured by the user by adjusting the relation of the optical bandwidth and dispersion of the fiber stretcher. Fundamentally, what limits the system parameters is the available optical energy and bandwidth, as well as the O/E converter (photodiode) sensitivity and electrical bandwidth. The relation between the RF time aperture and temporal resolution (time–bandwidth product) of the signal generator is determined by the number of independent control elements in the modulator used in the optical pulse shaper. Our current apparatus utilizes a 128-element modulator array, which sets the upper bound on the time–bandwidth product to 64. Given optical modulators with 640 independent elements are commercially available, the time-bandwidth product of the system could be easily scaled toward 320. With the typical power levels and optical bandwidths of communications-wavelength fiber lasers, a reasonable estimate of the longest time aperture would be ∼60 ns with a resolution determined by the optical modulator. As a reasonable estimate for the highest frequencies available, the use of high-speed unitraveling-carrier photodiodes [18] (though these are research devices for the moment) could extend this technique to greater than 100 GHz with the time aperture determined by the optical modulator.

A variety of waveforms, including ultra-broadband impulses, chirped sinusoids, and monocycles are achievable from our system, and several intriguing example waveforms are given in [10]. In Section II-B, we demonstrate how photonic synthesis techniques for arbitrary RF waveforms could have a significant impact on UWB RF systems by enabling precompensation for system distortions such as those arising from the nonideal phase response of certain broadband antennas.

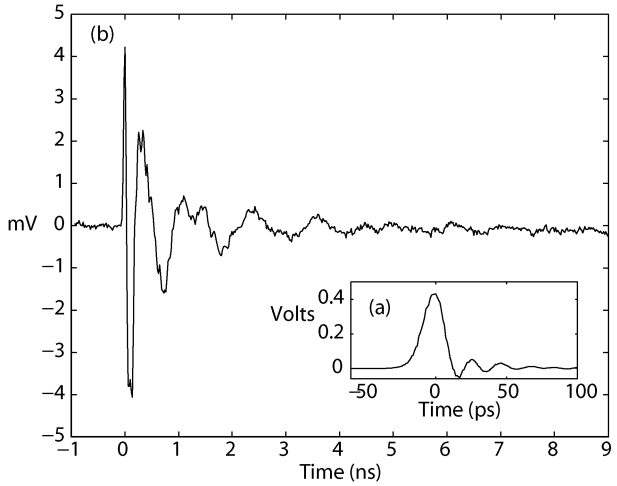

Fig. 2. (a) Photonically synthesized impulsive excitation waveform. (b) Measured impulse response of the ∼1-m antenna link.

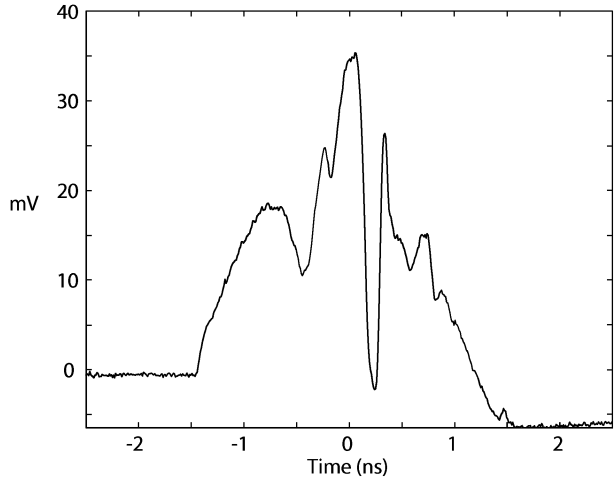

Fig. 3. Practical matched input signal obtained from our photonic time-domain electromagnetic waveform generator. To obtain this signal, a portion of the time-reversed system impulse response (Fig. 2) is sampled and programmed as the desired output from our waveform generator.

B. Compensation of Phase Distortions in Ridged TEM Horn Antennas

To characterize our antennas, we first obtain the impulse response $h(t)$ of the antenna link by exciting the transmit antenna with an ∼18-ps 400-mV peak voltage impulse derived directly from the laser output via the photodiode. The measured impulse response and driving impulse (inset) are shown in Fig. 2. Clearly, the short pulse input is dispersed; the received waveform shows clear oscillations over roughly 4 ns. Additionally, the received waveform is down-chirped with the low-frequency components near the antenna passband edge of ∼900 MHz occurring roughly 4 ns after the initial monocycle at the leading edge of the waveform. The large dispersion between the high-frequency (∼14 GHz) and low-frequency (∼900 MHz) components is attributed to the strong variations in the RF spectral phase near cutoff in the antenna.

Since the bandwidth of the input pulse (approximately $1/(2 \times$ pulsewidth) or ∼27 GHz) is significantly greater than the bandwidth of our antennas, we can effectively regard the waveform of Fig. 2 as the impulse response of the antenna link. From the Fourier transform of the impulse response, we are then able to extract the additional spectral phase contributed by the antenna pair. The received waveform may then be compressed to a short pulse, provided the input signal exhibits the opposite RF spectral phase to that arising from the antenna pair. So long as the input signal to the transmitting antenna maintains this particular spectral phase, the spectral amplitude may be also be tailored. For example, the spectral amplitude may be equalized to the minimize the pulsewidth of the received voltage waveform. Intuitively, the simplest optimized input waveform $x(t)$ that will produce an impulse upon reception is a signal "matched" to the antenna link, i.e., a time-reversed version of the impulse response

$$x(t) = h(-t). \tag{1}$$

Upon reception, the received voltage amplitude will then be given by the autocorrelation of the link impulse response

$$r(t) = h(t) * h(-t) \tag{2}$$

where $*$ denotes convolution. To illustrate the capability of our technique to mitigate antenna phase distortions, we focus on this matched-filter solution for the optimized input waveform.

To achieve an approximation to the matched signal for our system, the antenna system impulse response is sampled and a time-reversed version of the sampled waveform is applied as the optical spectral filter function in our photonic time-domain signal generator. The resulting electrical waveform $x(t) \approx h(-t)$ is shown in Fig. 3. Here, the practical matched signal shows a duration of ∼3 ns—roughly 75% of the duration of the impulse response—and is determined by the time aperture in our signal generator. Our system relies on the mapping of optical intensity to an electrical waveform, therefore, the resulting electrical signal is required to be a positive-definite quantity. This fact, along with the underlying shape of the optical power spectrum (manifested as the approximately Gaussian aperture of the electrical waveform) motivates us to choose the first 2 ns of the time-reversed impulse response as our desired electrical waveform. This ensures we retain the majority of the high-frequency content of the signal. The negative portion of the waveform, which occurs at times after roughly 1.2 ns, is the result of high-pass filtering effects in our electrical measurement.

Fig. 4(a) shows the measured received waveform when the practical matched signal is applied to the transmitting antenna. As expected, this waveform agrees quite well with the predicted response obtained from the convolution of the waveform in Fig. 3 with a scaled version of the link impulse response $(x(t) * h(t))$, shown in Fig. 4(b). To illustrate the ideally matched response, the calculated autocorrelation of the link impulse response $(h(t) * h(-t))$ is shown in Fig. 4(c). Note that the ideal response has been scaled to the same peak voltage value as Fig. 4(b) for ease of comparison. Upon comparison with the impulse response [see Fig. 2(b)], the received signal is visually more pulse-like in nature and shows significantly less oscillation after the main central peak. It should be noted that the peak amplitude of the received signal is roughly two times lower than the peak voltage in the impulsive drive experiment (Fig. 2); however, the practical matched input signal used in our experiment is an order of magnitude lower in peak voltage

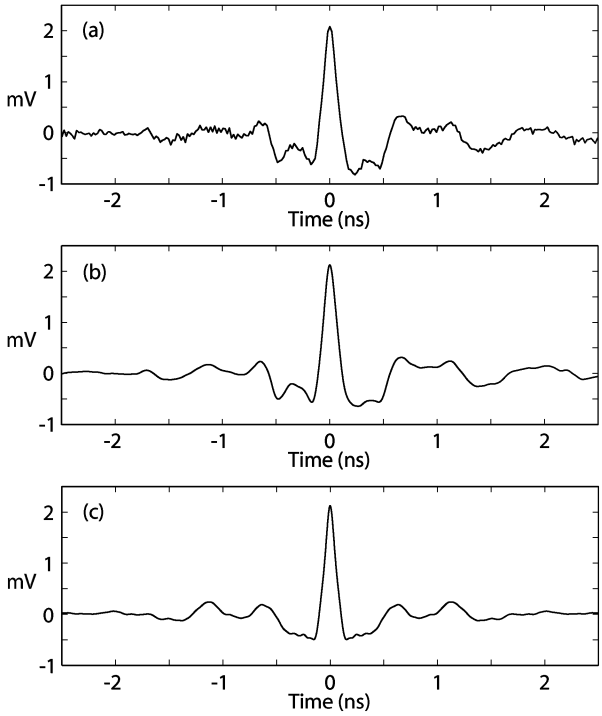

Fig. 4. (a) Measured link response when the practical matched input signal (Fig. 3) is applied to the transmitting antenna. (b) Predicted link response calculated by numerically convolving the practical matched input signal with the link impulse response. (c) Link response for the ideally matched input waveform.

than the impulsive input (40 mV versus 400 mV). The small late-time oscillations (beginning at ∼2 ns) are due to the fact that our practical matched signal only captures roughly the first 2 ns of the impulse response. Thus, the low-frequency components occurring outside this 2-ns aperture, though present in the practical matched waveform, are not phase compensated. These oscillations decay on the timescale of the initial impulse response (∼4 ns). This limitation also leads to the asymmetry in the waveforms of Fig. 4(a) and (b).

To quantify the compression of the received waveform, we focus on comparing properties of the normalized power defined as

$$P_N = \frac{|V_{\rm rec}|^2}{|V_{\rm in_{max}}|^2} \tag{3}$$

where $V_{\rm rec}$ is the received voltage waveform and $V_{\rm in_{max}}$ is the peak value of the input voltage waveform. The normalized powers for the impulse response, measured (practical) matched response, and (calculated) ideally matched response are shown in Fig. 5(a)–(c), respectively. In Fig. 5(b), the dashed curve illustrates the normalized power for the received waveform predicted from the link impulse response [see Fig. 2(b)] and the practical matched input waveform (Fig. 3). The three metrics we choose to define compression of the received signal are the peak normalized power, duration, and level of secondary oscillations in the received waveform compared to the main peak (sidelobe level). Comparison of the normalized power of the impulse response [see Fig. 5(a)] to that of the practical matched response [see Fig. 5(b)] clearly illustrates the gain in peak normalized power. The practical matched response exhibits a 36

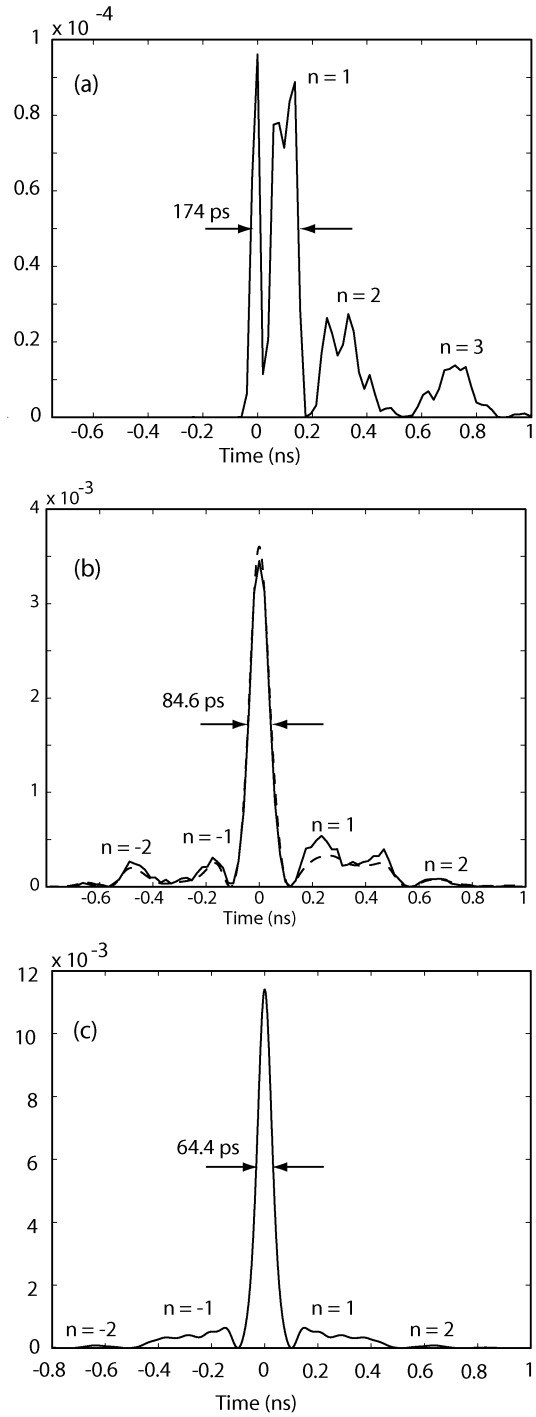

Fig. 5. Comparison of normalized power for the: (a) impulse response, (b) measured (practical) matched response (dashed curve is the normalized power predicted from the link response and practical matched input waveform), and (c) calculated ideally matched response. The measured matched response is clearly compressed relative to the impulse response; the measured matched response (b) exhibits a 36 times larger peak normalized power, approximately half the duration, and reduced secondary oscillations (sidelobes) compared to the impulse response (a). For comparison, the ideally matched response in (c) exhibits the expected temporal symmetry, maximized peak normalized power, and reduced temporal duration.

times larger peak power than the impulse response (recall that the peak received voltage for impulsive or matched excitation was approximately the same, whereas the practical matched input had an order-of-magnitude lower peak voltage value).

The pulsewidth—defined as the time interval over which any oscillations reach 50% of the peak normalized power—is also clearly shorter for the practical matched response. The duration of the practical matched response (∼85 ps) is essentially half that of the impulse response (∼174 ps). The practical matched response also compares well with the ideally matched response shown in Fig. 5(c). The ideally matched response shows a peak normalized power approximately three times greater than that of the practical matched response and a ∼18-ps reduction in duration. The increase in peak normalized power for the ideally matched response is larger than the ∼21% decrease in duration would suggest. This is largely explained by the unipolar nature of the practical matched input waveform, which is in contrast to the bipolar nature of the ideal matched waveform. Due to the required dc offset in the practical matched input waveform, the maximum voltage amplitude [$V_{\text{in}_{\max}}$ in (3)] is roughly twice that of the oscillatory signal component relevant to our experiments. In addition, the practical matched input signal exhibits a slightly lesser bandwidth than the ideally matched waveform.

Another (perhaps more insightful) metric that can be used to describe how well a signal is matched to a particular system is the ratio of the normalized power of the secondary oscillations to that of the largest (main) oscillation in the received signal. This metric is analogous to comparing the power in the main beam of an antenna array to the power in the sidelobes. We define the sidelobe level for our signals to be

$$S = 10\log_{10}\frac{|V_n|^2}{|V_p|^2}\,(\text{dB}) \tag{4}$$

where $|V_n|$ is the voltage magnitude of the nth secondary oscillation and $|V_p|$ is the voltage magnitude of the largest oscillation. The rate at which the sidelobes decay is a measure of energy concentration in the time domain—more of the total waveform energy is concentrated in the central peak as the sidelobes decay more rapidly. Table I summarizes this comparison. Note that the sidelobe levels for the ideally matched response [see Fig. 5(c)] are given in parentheses. The sidelobe levels for the practical matched response, when compared to those of the impulse response, show a dramatic improvement. Though the practical matched input signal is only an approximation to the ideal matched signal, the $n = 1$ oscillation in the practical response has been pushed down to approximately the level of the $n = 3$ sidelobe in the impulse response; all other oscillations in the practical matched response have been pushed well below this level. The sidelobe levels of the practical matched response also compare reasonably well with the ideal response, particularly the levels of the $n = +/-1$ sidelobes, which are within 4.4 and 2.0 dB of the ideal levels, respectively. This discrepancy in the sidelobe levels arises due to the time-aperture limitation of our waveform generator.

With regard to UWB systems in general, the primary capability of our photonic time-domain electromagnetic waveform generator is that it enables arbitrary user-defined temporal waveforms with frequency content throughout the 3.1–10.6-GHz UWB band. Such bandwidth and waveform agility is, to our knowledge, not offered from available reprogrammable electronic pulse formers. We note, this proof-of-concept matched-filtering example utilizes a baseband waveform. Therefore, the signals illustrated here exhibit low-frequency content outside of the above UWB frequency band. This low-frequency content can be removed by utilizing amplitude-modulated impulses; compression may still be achieved given the knowledge of RF spectral phase acquired from the measurement of the link impulse response. As our waveform generator currently exhibits an RF bandwidth of approximately 11 GHz, amplitude-modulated impulses with frequency content in the above band may be synthesized—several example waveforms demonstrating this capability are given in [19]. To address spectral emission limits for UWB systems applications—specifically, emission limits for frequencies below 3.1 GHz—apodization of the desired time-domain waveforms may be incorporated in our apparatus, along with an electronic high-pass filter, to remove low-frequency content.

TABLE I
COMPARISON OF SIDELOBE LEVELS IN THE RECEIVED WAVEFORM FOR IMPULSIVE AND PRACTICAL MATCHED EXCITATION

Signal	Sidelobe #	Position (ns)	S (dB)
Matched	n = -2	-0.5	-11.1 (-21.3)
	n = -1	-0.18	-10.5 (-12.5)
	n = 1	0.23	-8.1 (-12.5)
	n = 2	0.68	-16.1 (-21.3)
Impulse	n = 1	0.135	-0.3
	n = 2	0.331	-5.4
	n = 3	0.71	-8.5

III. CONCLUSION

In conclusion, we have experimentally demonstrated a technique for reprogrammable compensation of antenna dispersion in UWB RF systems. Our technique, which exploits photonic-synthesis techniques for arbitrary electromagnetic waveforms, enables the conjugate antenna phase response to be applied directly to the transmit waveform in a UWB system. Though the study presented here focuses on the matched-filter solution for phase compensation, we note that we are working to extend our technique to other UWB optimized waveforms—e.g., waveforms designed to mitigate the $1/f^2$ frequency dependence of the received power inherent in a wireless link or to account for gain variations in the antennas. In addition, we are currently investigating the dispersive behavior of other broadband antenna structures and the applicability of our technique for phase compensation in these structures.

ACKNOWLEDGMENT

The authors would like to thank graduate student H. Quixada, Purdue University, West Lafayette, IN, for performing frequency-domain measurements on the antennas and Prof. W. Chappell, Purdue University, for use of the vector network analyzer and laboratory space for the frequency-domain measurements.

REFERENCES

[1] C. Lim, A. Nirmalathas, D. Novak, R. Waterhouse, and G. Yoffe, "Millimeter-wave broad-band fiber-wireless system incorporating baseband data transmission over fiber and remote LO delivery," *J. Lightw. Technol.*, vol. 18, no. 10, pp. 1355–1363, Oct. 2000.

[2] P. W. Juodawlkis, J. C. Twichell, G. E. Betts, J. J. Hargreaves, R. D. Younger, J. L. Wasserman, F. J. O'Donnell, K. G. Ray, and R. C. Williamson, "Optically sampled analog-to-digital converters," *IEEE Trans. Microw. Theory Tech.*, vol. 49, no. 10, pp. 1840–1853, Oct. 2001.

[3] A. S. Bhushan, P. V. Kelkar, B. Jalali, O. Boyraz, and M. Islam, "130-GSa/s photonic analog-to-digital converter with time stretch preprocessor," *IEEE Photon. Technol. Lett.*, vol. 14, no. 5, pp. 684–686, May 2002.

[4] T. Yilmaz, C. M. DePriest, T. Turpin, J. H. Abeles, and P. J. Delfyett, "Toward a photonic arbitrary waveform generator using a modelocked external cavity semiconductor laser," *IEEE Photon. Technol. Lett.*, vol. 14, no. 11, pp. 1608–1610, Nov. 2002.

[5] J. D. McKinney, D. S. Seo, D. E. Leaird, and A. M. Weiner, "Photonically assisted generation of arbitrary millimeter-wave and microwave electromagnetic waveforms via direct space-to-time optical pulse shaping," *J. Lightwave Technol.*, vol. 21, no. 12, pp. 3020–3028, Dec. 2003.

[6] M. Z. Win and R. A. Scholtz, "Ultra-wide bandwidth time-hopping spread-spectrum impulse radio for wireless multiple-access communications," *IEEE Trans. Commun.*, vol. 48, no. 4, pp. 679–691, Apr. 2000.

[7] J. S. Lee, C. Nguyen, and T. Scullion, "A novel, compact, low-cost, impulse ground-penetrating radar for nondestructive evaluation of pavements," *IEEE Trans. Instrum. Meas.*, vol. 53, no. 6, pp. 1502–1509, Dec. 2004.

[8] "First report and order (revision of part 15 of the Comission's rules regarding ultra-wideband transmission systems)," FCC, Washington, DC, eT Docket 98-153, adopted February 14, 2002, released April 22, 2002.

[9] J. Chou, Y. Han, and B. Jalali, "Adaptive RF-photonic arbitrary waveform generator," *IEEE Photon. Technol. Lett.*, vol. 15, no. 4, pp. 581–583, Apr. 2003.

[10] I. Lin, J. D. McKinney, and A. M. Weiner, "Photonic synthesis of broadband microwave arbitrary waveforms applicable to ultra-wideband communication," *IEEE Microw. Wireless Compon. Lett.*, vol. 15, no. 4, pp. 226–228, Apr. 2005.

[11] D. Lamensdorf and L. Susman, "Baseband-pulse-antenna techniques," *IEEE Antennas Propag. Mag.*, vol. 36, no. 1, pp. 20–30, Feb. 1994.

[12] A. Shlivinski, E. Heyman, and R. Kastner, "Antenna characterization in the time domain," *IEEE Trans. Antennas Propag.*, vol. 45, no. 7, pp. 1140–1149, Jul. 1997.

[13] J. H. Reed, Ed., *An Introduction to Ultra Wideband Communication Systems*. Upper Saddle River, NJ: Prentice-Hall, 2005.

[14] D. M. Pozar, R. E. McIntosh, and S. G. Walker, "The optimum feed voltage for a dipole antenna for pulse radiation," *IEEE Trans. Antennas Propag.*, vol. AP-31, no. 4, pp. 563–569, Jul. 1983.

[15] D. M. Pozar, Y.-W. Kang, D. H. Schaubert, and R. E. McIntosh, "Optimization of the transient radiation from a dipole array," *IEEE Trans. Antennas Propag.*, vol. AP-33, no. 1, pp. 69–75, Jan. 1985.

[16] D. M. Pozar, "Waveform optimizations for ultrawideband radio systems," *IEEE Trans. Antennas Propag.*, vol. 51, no. 9, pp. 2335–2345, Sep. 2003.

[17] A. M. Weiner, "Femtosecond pulse shaping using spatial light modulators," *Rev. Sci. Instrum.*, vol. 71, pp. 1929–1960, 2000.

[18] H. Ito, S. Kodama, Y. Muramoto, T. N. Tomofumi Furuta, and T. Ishibashi, "High-speed and high-output InP–InGaAs unitraveling-carrier photodiodes," *IEEE J. Sel. Topics Quantum Electron.*, vol. 10, no. 4, pp. 709–727, Jul.–Aug. 2004.

[19] J. D. McKinney, I. S. Lin, and A. M. Weiner, "Engineering of the radio-frequency spectra of ultrawideband electromagnetic waveforms via optical pulse shaping techniques," in *Int. Microw. Photon. Top. Meeting*, Ogunquit, ME, Oct. 4–6, 2004, pp. 81–84.

Jason D. McKinney (M'03) received the Ph.D. degree in electrical engineering from Purdue University, West Lafayette, IN, in 2003.

From July 2001 to May 2003, he was a Graduate Assistance in Areas of National Need (GAANN) Fellow, during which time he was active in both teaching and research at Purdue University. His doctoral research included the first demonstration of ultrafast optical pulse-shaping techniques for synthesis of arbitrarily-shaped millimeter waveforms exhibiting arbitrary phase and frequency modulation at center frequencies up to 50 GHz. Upon completion of the doctoral degree, he was a Visiting Assistant Professor (2003–2005) with the School of Electrical and Computer Engineering, Purdue University, where he is currently a Research Scientist. He is an Associate Fellow of the Purdue University Teaching Academy. His research interests include ultrafast optical pulse processing and applications of photonics in microwave systems.

Dr. McKinney is a member of the Optical Society of America (OSA). He was the recipient of various awards for his research, most notably the 2003 Chorafas Prize for doctoral research (awarded to one Purdue doctoral student per year) and as a finalist for the 2002 Optical Society of America/New Focus Student Award. He was also the recipient of numerous awards in recognition of his teaching.

Andrew M. Weiner (F'95) received the Sc.D. degree in electrical engineering from the Massachusetts Institute of Technology (MIT), Cambridge, in 1984.

From 1979 to 1984, he was a Fannie and John Hertz Foundation Graduate Fellow with MIT. Upon graduation, he joined Bellcore, initially as a Member of Technical Staff and then as Manager of ultrafast optics and optical signal processing research. In 1992, he joined Purdue University, West Lafayette, IN, where he is currently the Scifres Distinguished Professor of Electrical and Computer Engineering. From 1997 to 2003, he was the Electrical and Computer Engineering (ECE) Director of Graduate Admissions. He has authored five book chapters and over 160 journal papers and coedited one book. He has also authored or coauthored over 300 conference papers, 80 conference invited talks, and has presented over 70 additional invited seminars at university, industry, and government organizations. He holds eight U.S. patents. His research focuses on ultrafast optical signal processing and high-speed optical communications. He is especially well known for pioneering the field of femtosecond pulse shaping, which enables generation of nearly arbitrary ultrafast optical waveforms according to user specification.

Prof. Weiner is a Fellow of the Optical Society of America (OSA). He was the recipient of numerous awards for his research including the 1984 Hertz Foundation Doctoral Thesis Prize, the 1990 Adolph Lomb Medal of the Optical Society of America awarded for pioneering contributions to the field of optics made before the age of thirty, the 1997 Curtis McGraw Research Award of the American Society of Engineering Education, the 1997 International Commission on Optics Prize, the 1999 IEEE Lasers and Electro-Optics Society (IEEE LEOS) William Streifer Scientific Achievement Award, the 2000 Alexander von Humboldt Foundation Research Award for Senior U.S. Scientists, and the inaugural 2003 Research Excellence Award from the Schools of Engineering at Purdue.